JOURNAL OF PROPULSION AND POWER
Vol. 22, No. 1, January–February 2006

Low Heating Value Fuel Combustion: Flamelet Combustion Model and NO Formation Model

Takahisa Yamamoto*
Toyohashi University of Technology, Toyohashi 441-8580, Japan
and
Tomohiko Furuhata†
Gunma University, Kiryu 376-8515, Japan

This study has performed the numerical simulations of turbulent low-heating-value fuel (LHVF) combustion and NO emissions using a flamelet model and a newly developed NO formation model. The emphases of this study are that the flamelet model employs a flamelet library specialized to LHVF combustion reaction, and a NO formation model involves not only the Zeldovich mechanism but also Fenimore mechanism. The calculated results of temperature and chemical species concentrations are compared with the measured ones. In consequence, it is clarified that the flamelet model can predict temperature and chemical species distributions of experimental results well, and the NO formation model developed in this paper shows good agreement with experimental results quantitatively.

Nomenclature

C_{g1}, C_{g2}	=	g-equation model constants
C_μ, $C_{\epsilon 1}$, $C_{\epsilon 2}$	=	k-ϵ model constants
D	=	combustor diameter, m
F_x, F_r, F_θ	=	composite radiation flux, W/m^2
f	=	mixture fraction
G_k	=	stress production of k, m^2/s^3
g	=	variance of mixture fraction f
h	=	enthalpy, kJ/kg
k	=	turbulent kinetic energy, m^2/s^2
L	=	distance between jet planes, m
m_i	=	mass fraction for specie i
P	=	pressure, Pa
$\mathcal{P}$	=	probability density function
S_ϕ	=	source term of dependent variable ϕ
U, V, W	=	time mean velocity components, m/s
v_P	=	prompt NO reaction rate, mole/(m^3 s)
v_T	=	thermal NO reaction rate, mole/(m^3 s)
X_i	=	mole fraction of specie i
x, r, θ	=	cylindrical coordinate
Z_i	=	mass fraction of element i
Γ_ϕ	=	diffusion coefficient for ϕ
ϵ	=	dissipation rate of k, m^2/s^3
μ	=	viscosity, Pa · s
ρ	=	density, kg/m^3
σ_k, σ_ϵ, σ_m, σ_h, σ_f, σ_g	=	effective Schmidt numbers
ϕ	=	dependent variable
χ	=	scalar dissipation rate, 1/s

Subscripts

P	=	prompt NO
T	=	thernam NO

Received 15 March 2004; revision received 31 May 2005; accepted for publication 26 May 2005. Copyright © 2005 by the American Institute of Aeronautics and Astronautics, Inc. All rights reserved. Copies of this paper may be made for personal or internal use, on condition that the copier pay the $10.00 per-copy fee to the Copyright Clearance Center, Inc., 222 Rosewood Drive, Danvers, MA 01923; include the code 0748-4658/06 $10.00 in correspondence with the CCC.

*Ph.D., Department of Mechanical Engineering, 1-1 Hibarigaoka, Tenpaku-cho; taka@mech.tut.ac.jp.
†Ph.D., Department of Mechanical Engineering, 1-5-1 Tenjin-cho.

Introduction

LOW-HEATING-VALUE fuel (LHVF), which is composed of CH_4, H_2, CO, CO_2, and minor components like NH_3, is mainly produced from coal and biomass gasification processes and blast furnaces in steel plants. Recently, LHVF received worldwide attention as a new energy resources, and it is being studied to use LHVF as a fuel in gas turbine systems.[1] Because major pollutants such as sulfur content and heavy trace metals are already eliminated in the gasification process, LHVF can be used as a clean combustion fuel similar to natural gas. The authors propose a new-concept LHVF gas turbine system[2,3] that employs a combination of fuel-rich and fuel-lean combustion processes. In previous studies, the authors performed thermodynamic and exergy analysis of the proposed system and estimated its power generation efficiency to be over 60% (Refs. 4 and 5). One of the tasks in developing this system is to design a gas turbine combustor specialized for the LHVF and to predict environmental pollutant emissions such as nitrogen oxides.

In this study, we developed a numerical combustion model and a NO formation model specialized for the field of turbulent LHVF combustion. One of the focus areas of this study is to develop a LHVF combustion simulation model and NO formation model for "industrial and practical uses." In other words, the models developed in this study were required to be cheap and consume less CPU time. Hence, in this study a k-ϵ two-equation model and a flamelet combustion model were used for the turbulent flow and turbulent combustion models. Coupling calculation using a large-eddy-simulation model for turbulent flow and the detailed chemical reaction model (e.g., 50 chemical species and 300 elementary reactions) for chemical reactions yields more accurate results for an LHVF gas turbine combustor.[6–8] However, such a calculation requires much more CPU power and time, which makes it unsuitable for industrial and practical uses.[9–13] In addition, almost all NO formation simulation studies performed thus far took into account only the Zeldovich (thermal) NO mechanism, while the Fenimore (prompt) NO mechanism was not taken into account. Thus, the NO formation model involving both the Zeldovich NO and Fenimore NO mechanisms was recently developed here.

This study carried out LHVF turbulent combustion experiments for both the models under the same conditions, and the results were compared. Further, the flamelet model with the flamelet library specialized for the LHVF and the NO formation model were compared and evaluated their accuracy.

Table 1 Chemical components of LHVF[2,3,14,15]

Chemical component	Vol., %
CH_4	11.0
N_2	50.0
CO_2	10.0
H_2	15.0
CO	14.0

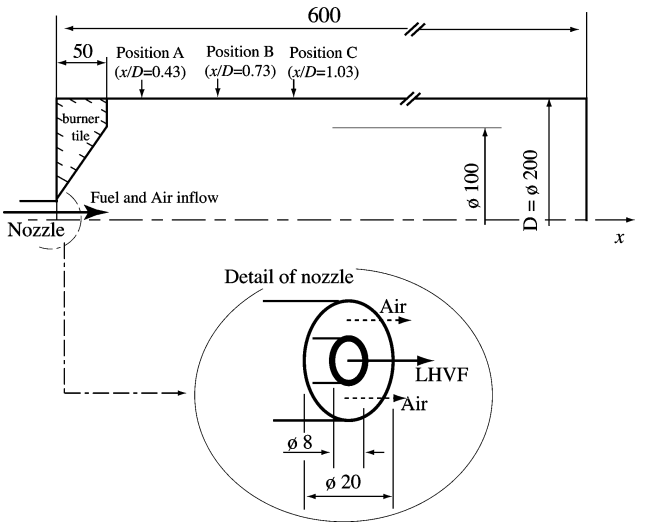

Fig. 1 Schematic drawing of turbulent LHVF combustor.

Experimental

To evaluate the accuracy of the numerical simulation model, experiments on LHVF turbulent combustion were carried out. Figure 1 shows the details of a test combustor used in this study.

The size of the combustor is as follows: inner diameter, 200 mm; and length, 600 mm. The combustor is made of stainless steel, and a coaxial-type fuel/air injector is employed. The fuel enters the combustor through a inner nozzle (ϕ 8 mm) of an injector, and air enters through the outer swirler nozzle (ϕ 20 mm), which is fitted at an angle of 30 deg.

The composition of LHVF is as shown in Table 1. The composition of this syngas refers to our previous studies[2–4] and the references of coal and biomass gasification studies.[14,15] The fuel and air feed rates are set to 37 and 64 l/min, respectively. Then the Reynolds number based on the outlet of the fuel injector is 5011, swirl number is 0.33, and equivalence ratio is 0.8. An atmospheric pressure is maintained in the combustor. Combustion gas temperature and species compositions are measured at three positions. Positions A, B, and C are located at 86 ($x/D = 0.43$), 146 ($x/D = 0.73$), and 206 mm ($x/D = 1.03$), respectively, where x is the axial distance and D is the inner diameter. At each position, the R type (Pt/Pt-Rh 16%) thermocouples with a 0.1-mm wire diameter are set at 17 points (at intervals of 5 mm) in the radial direction of the combustor. The sampling rate of the temperature measurement is set at 500 Hz, taking into account the response time of the thermocouple, and the radiation loss of the thermocouple is eliminated by using a suction pyrometer unit. Gases are sucked through a water-cooled sampling probe made of stainless steel at six points (at an interval of 10 mm) in the radial direction. The tip diameter of the gas sampling probe is ϕ 1 mm. Intensive cooling starts at the joint of the probe tip by a water jacket cooling system where chemical reactions halt. Sampling gases are analyzed by using a gascromatograph with a thermal conductivity detector and chemiluminescence analyzer. These measurements were carried out for a duration of 1 min, and the measured data were converted to time average data. The deviations in the tempereture and the concentrations of the chemical specie in the experiment are approximately 5 and 3% from the time-averaged data, respecetively.

Outline of the Turbulent LHVF Combustion Simulation

Combustion Flowfield

The numerical simulation of the flowfield includes a solution of the overall continuity equation and the Navier–Stokes equations in low-Mach-number formulation. The turbulent flow is described by the standard k-ϵ two-equations model,[16] and radiative heat transfer is calculated by using the six-flux radiative heat-transfer model.[17] The generalized conservation equation in three-dimensional cylindrical coordinates for a dependent variable ϕ is

$$\frac{\partial}{\partial x}(\rho U\phi) + \frac{1}{r}\frac{\partial}{\partial r}(r\rho V\phi) + \frac{1}{r}\frac{\partial}{\partial \theta}(\rho W\phi) = \frac{\partial}{\partial x}\left(\Gamma_\phi \frac{\partial \phi}{\partial x}\right) + \frac{1}{r}\frac{\partial}{\partial r}\left(r\Gamma_\phi \frac{\partial \phi}{\partial r}\right) + \frac{1}{r}\frac{\partial}{\partial \theta}\left(\Gamma_\phi \frac{\partial \phi}{r\partial \theta}\right) + S_\phi \tag{1}$$

The dependent variable ϕ represents mass (continuity); momentum (U, V, W); turbulence energy k, the dissipation rate of the turbulence energy ϵ; enthalpy h; radiative heat flux F_x, F_r, F_ϕ; mixture fraction f; and the variance of mixture fraction g. Γ_ϕ is the turbulent diffusive coefficient, and S_ϕ is the source term. The expressions for the source terms are shown in Table 2. The governing equations are iteratively solved by using the SIMPLE (Semi-Implicit Method for Pressure-Linked Equation) algorithm with TDMA (Tri-Diagonal Matrix Algorithm).[18] This study surveyed the effect of a number of grid nodes and consequently employed three-dimensional, cylindrical, finite-difference grid that has $65 \times 60 \times 4$ grid nodes in the axial, radial, and angular directions, respectively.

Flamelet Model

In the turbulent combustion simulation, eddy dissipation concept (EDC) is one of the currently used models for two reasons: 1) this model expresses the reaction rate as a simple proportionality relation, that is, the mass fractions of the fuel and oxidant and the characteristic time of eddy dissipation ϵ/k; and 2) this model simplifies the actual reactions into a few overall reactions, for example, the complicated methane combustion mechanism is reduced to one reaction $CH_4 + 2O_2 \rightarrow CO_2 + 2H_2O$. The drawback of this model is the unsuitability to combustion of synthetic fuels like LHVF; the chemical reaction mechanisms and combustion characteristics completely depend on the concentrations of chemical species such as CH_4, H_2, and CO. This study, therefore, focused on employing the flamelet model for the turbulent combustion model. The concept of the flamelet model can be considered as an extension of the "flame sheet" model that assumes an infinitely fast chemical reaction such that the reaction zone has an infinitely thin interface.[19] Assuming equal diffusivity under constant-pressure combustion without heat losses, the thermochemical properties are completely determined by a local mixing state, which is described by the mixture fraction f:

$$f = \frac{Z_i - Z_{i,\text{air}}}{Z_{i,\text{fuel}} - Z_{i,\text{air}}} \tag{2}$$

where $Z_{i,\text{fuel}}$ denotes the mass fraction of element i in the mixture originating from the fuel stream and $Z_{i,\text{air}}$ denotes the mass fraction of element i in the mixture originating from the airstream. The flamelet concept introduces a scalar dissipation rate χ that describes the degree of departure from equilibrium state and can be interpreted as the inverse of characteristic diffusion time. Under the condition of widely separated timescales, the combustion chemistry reaches a quasi steady state and immediately adjusts to the local flow condition. By transformation of the physical coordinate into ones using the mixture fraction, the temperature and species are determined from the balance between the diffusion and chemical reaction as

$$\rho \frac{1}{Le}\frac{\chi}{2}\frac{\mathrm{d}^2 T}{\mathrm{d}f^2} = \frac{(-\Delta h)}{C_p}\sum \omega_i \tag{3}$$

where Le is Lewis number and is set at unity ω_i is the mass production rate of the chemical specie i, and χ is the scalar dissipation rate and is defined as follows[20,21]:

$$\chi = C_\chi(\epsilon/k)g^2 \tag{4}$$

where C_χ is set equal 2.0.

Table 2 Source terms and turbulent diffusion coefficients for governing equations

Variable	ϕ	Γ_ϕ	S_ϕ
Mass	1	0	0
Axial momentum	U	μ_{eff}	$\frac{\partial}{\partial x}\left(\mu_{\text{eff}}\frac{\partial U}{\partial x}\right)+\frac{1}{r}\frac{\partial}{\partial r}\left(r\mu_{\text{eff}}\frac{\partial V}{\partial r}\right)+\frac{1}{r}\frac{\partial}{\partial \theta}\left(\mu_{\text{eff}}\frac{\partial W}{\partial x}\right)-\frac{\partial P}{\partial x}$
Radial momentum	V	μ_{eff}	$\frac{\partial}{\partial x}\left(\mu_{\text{eff}}\frac{\partial U}{\partial r}\right)+\frac{1}{r}\frac{\partial}{\partial r}\left(r\mu_{\text{eff}}\frac{\partial V}{\partial r}\right)+\frac{1}{r}\frac{\partial}{\partial \theta}\left[r\mu_{\text{eff}}\frac{\partial}{\partial r}\left(\frac{W}{r}\right)\right]$ $-2\frac{\mu_{\text{eff}}}{r}\left(\frac{\partial W}{r\partial\theta}+\frac{V}{r}\right)+\frac{\rho W^2}{r}-\frac{\partial P}{\partial r}$
Tangential momentum	W	μ_{eff}	$\frac{\partial}{\partial x}\left(\mu_{\text{eff}}\frac{\partial U}{r\partial\theta}\right)+\frac{\mu_{\text{eff}}}{r}\left[r\frac{\partial}{\partial r}\left(\frac{W}{r}\right)+\frac{1}{r}\frac{\partial V}{\partial\theta}\right]+\frac{1}{r}\frac{\partial}{\partial r}\left[r\mu_{\text{eff}}\left(\frac{1}{r}\frac{\partial V}{\partial\theta}-\frac{W}{r}\right)\right]$ $+\frac{1}{r}\frac{\partial}{\partial\theta}\left[\mu_{\text{eff}}\left(\frac{\partial W}{r\partial\theta}+\frac{2V}{r}\right)\right]-\rho\frac{VW}{r}-\frac{\partial P}{r\partial\theta}$
Kinetic energy	k	$\mu_{\text{eff}}/\sigma_k$	$G_k-\rho\epsilon$
Dissipation rate	ϵ	$\mu_{\text{eff}}/\sigma_\epsilon$	$\frac{\epsilon}{k}(C_{\epsilon1}G_k-C_{\epsilon2}\rho\epsilon)$
Stagnation enthalpy	h	$\mu_{\text{eff}}/\sigma_h$	$2a_R(F_x+F_r+F_\theta-3E)$
Mixture fraction	f	$\mu_{\text{eff}}/\sigma_f$	0
Concentration fluctuation	g	$\mu_{\text{eff}}/\sigma_g$	$C_{g1}G_g-C_{g2}\rho\frac{\epsilon}{k}$
Turbulent viscosity	——	——	$\mu_t=C_\mu\rho k^2/\epsilon$ ($C_\mu=0.9$)
Effective viscosity	——	——	$\mu_{\text{eff}}=\mu_t+\mu$

Table 3 Elementary reactions used in counterdiffusion flame calculation[27,28] [$k_i = B_i T^{\alpha_i}\exp(-E_i/RT)$][a]

No.		B_f[b]	α_f	E_f	B_b[b]	α_b	E_b
R1	$H+O_2\rightleftharpoons OH+O$	2.0×10^{14}	0.0	16,800.0	1.575×10^{13}	0.0	690.0
R2	$O+H_2\rightleftharpoons OH+H$	1.8×10^{10}	1.0	8,826.0	8.0×10^{9}	1.0	6,760.0
R3	$H_2+OH\rightleftharpoons H_2O+H$	1.170×10^{9}	1.3	3,626.0	5.090×10^{9}	1.3	18,588.0
R4	$OH+OH\rightleftharpoons O+H_2O$	6.0×10^{8}	1.3	0.0	5.9×10^{9}	1.3	17,029.0
R5	$H+O_2+M\rightarrow HO_2+M$	2.3×10^{18}	−0.8	0.0	——	——	——
R6	$H+HO_2\rightarrow OH+OH$	1.5×10^{14}	0.0	1,004.0	——	——	——
R7	$H+HO_2\rightarrow H_2+O_2$	2.5×10^{13}	0.0	700.0	——	——	——
R8	$OH+HO_2+M\rightarrow H_2O+O_2$	2.0×10^{13}	0.0	1,000.0	——	——	——
R9	$CO+OH\rightleftharpoons CO_2+H$	1.510×10^{7}	1.3	−758.0	1.570×10^{9}	1.3	22,337.0
R10	$CH_4+(M)\rightleftharpoons CH_3+H+(M)$	6.3×10^{14}	0.0	104,000.0	5.2×10^{12}	0.0	−1,310.0
R11	$CH_4+H\rightleftharpoons CH_3+H_2$	2.2×10^{4}	3.0	8,750.0	9.570×10^{2}	3.0	8,750.0
R12	$CH_4+OH\rightleftharpoons CH_3+H_2O$	1.6×10^{6}	2.1	2,460.0	3.020×10^{5}	2.1	17,422.0
R13	$CH_3+O\rightarrow CH_2O+H$	6.8×10^{13}	0.0	0.0	——	——	——
R14	$CH_2O+H\rightarrow HCO+H_2$	2.5×10^{13}	0.0	3,991.0	——	——	——
R15	$CH_2O+OH\rightarrow HCO+H_2O$	3.0×10^{13}	0.0	1,195.0	——	——	——
R16	$HCO+H\rightarrow CO+H_2$	4.0×10^{13}	0.0	0.0	——	——	——
R17	$HCO+M\rightarrow CO+H+M$	1.6×10^{14}	0.0	14,700.0	——	——	——
R18	$CH_3+O_2\rightarrow CH_3O+O$	7.0×10^{12}	0.0	25,652.0	——	——	——
R19	$CH_3O+H\rightarrow CH_2O+H_2$	2.0×10^{13}	0.0	0.0	——	——	——
R20	$CH_3O+M\rightarrow CH_2O+H+M$	2.4×10^{13}	0.0	28,812.0	——	——	——
R21	$HO_2+HO_2\rightarrow H_2O_2+O_2$	2.0×10^{12}	0.0	0.0	——	——	——
R22	$H_2O_2+M\rightleftharpoons OH+OH+M$	1.3×10^{17}	0.0	45,500.0	9.860×10^{14}	0.0	−5,070.0
R23	$H_2O_2+OH\rightleftharpoons H_2O+HO_2$	1.0×10^{13}	0.0	1,800.0	2.860×10^{13}	0.0	32,790.0
R24	$OH+H+M\rightarrow H_2O+M$	2.2×10^{22}	−2.0	0.0	——	——	——
R25	$H+H+M\rightarrow H_2+M$	1.8×10^{18}	−1.0	0.0	——	——	——

[a]Units are [mol], [cm^3], [s], [K], and [cal/mol]. [b]Subscripts f and b denote forward and backward reactions.

For the flamelet model, the local composition is determined by the relationship between the local values of the mixture fraction and the scalar dissipation rate. This relationship is referred to as a flamelet library. Unless the formation of these relationships is clear, the flamelet model cannot carry out the turbulent combustion simulation. However, the flamelet library specialized for the LHVF has not yet been studied and reported. This study has devised a new method to construct a flamelet library using the numerical simulation of counterflow diffusion flame. Its details are stated in the next section. Finally, the mean mass fraction of the chemical species is calculated using the probability density functions (PDFs):

$$\bar{m}_i = \int m_i(f,\chi)\mathcal{P}(f,\chi)\,\mathrm{d}\chi\,\mathrm{d}f \tag{5}$$

where f and χ are assumed to be statistically independent of each other, and then the PDF $\mathcal{P}(f,\chi)$ is calculated as follows[22,23]:

$$\mathcal{P}(f,\chi)=\mathcal{P}(f)\cdot\mathcal{P}(\chi) \tag{6}$$

A clipped Gaussian PDF and log-normal PDF have been employed for the mixture fraction and scalar dissipation rate.[24,25]

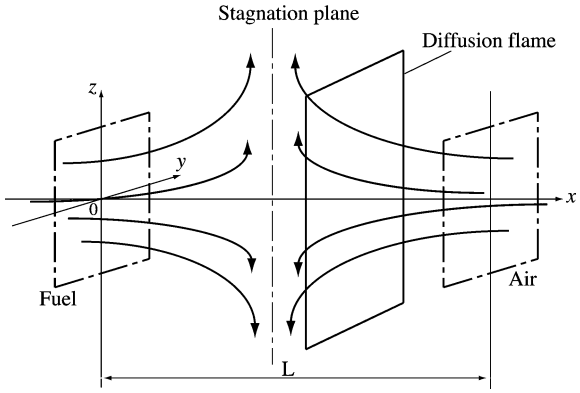

Fig. 2 Counterflow diffusion flame.[26]

LHVF Flamelet Library

This study proposes a method using the numerical simulation of counterflow diffusion flame to construct the flamelet library specialized for LHVF.

Figure 2 shows the analysis model of the counterflow diffusion flame.[26] Fuel and air-jet planes are situated at intervals of L. Each plane is infinitely wide in the y and z directions. Fuel and air are supplied at $x = 0$ and $x = L$, respectively. In this numerical simulation, L is set to 15 mm, and the number of differential grids in a computational domain are 201. Initial temperatures of both fuel and air are set at 298 K.

Table 3 shows a reaction mechanism used in the calculation of the counterflow diffusion flame that has 16 chemical species and 25 elementary reactions. This reaction mechanism has been discussed extensively by Bendtsen et al.[27] and Fujiwara et al.[28] Thermodynamic data for chemical reactions have been quoted from the CHEMKIN database.[29] Transport coefficients are calculated by using the simplified transport model.[30]

Figure 3 shows examples of the calculated results of the counterflow diffusion flame. When fuel and air inlet velocities are set at 1) 0.2 m/s, 2) 1.0 m/s, and 3) 3.0 m/s, the scalar dissipation rates are 0.81 1/s, 3.37 1/s, and 20.5 1/s, respectively. The width of the flame (reaction) zone is strongly affected by the inlet velocities and in turn by the scalar dissipation rate. The LHVF counterflow diffusion flame in this simulation blew off as high as over the scalar dissipation rate of 300 1/s. According to the reports by other researches,[26,28] the extinction limit of methane couterflow diffusion flame is found to be approximately in the range of 35 and 60 1/s. LHVF has extremely good flammability, as compared with the methane extinction limit.

By expressing the results of the counterflow diffusion flame in terms of the mixture fraction f, we can obtain the flamelet library of the LHVF combustion, as shown in Fig. 4. The library implies that the chemical species are functions of the mixture fraction f and scalar dissipation rate χ. In the calculation of a turbulent combustion field, the mixture fraction and scalar dissipation rate are estimated by flowfield calculation, and consequently, the chemical species concentration in each local position is determined by the library. One of the features of the flamelet model is the separation of the combustion reaction calculations from that of the flowfield.

NO Formation Model

The NO formation mechanism is very complicated, for example, in methane combustion, the transport equations for approximately 50 chemical species and over 300 elementary reactions are required for the exact simulation of NO formation.[26] Therefore, it is not realistic to carry out NO formation calculations with detailed chemical reactions by turbulent combustion simulation. This paper aimed some reaction routes of NO formation and described the NO formation model. The purpose of this model is to facilitate the calculations of the Zeldovich mechanism as well as Fenimore mechanism. The details of the model are explained as follows.

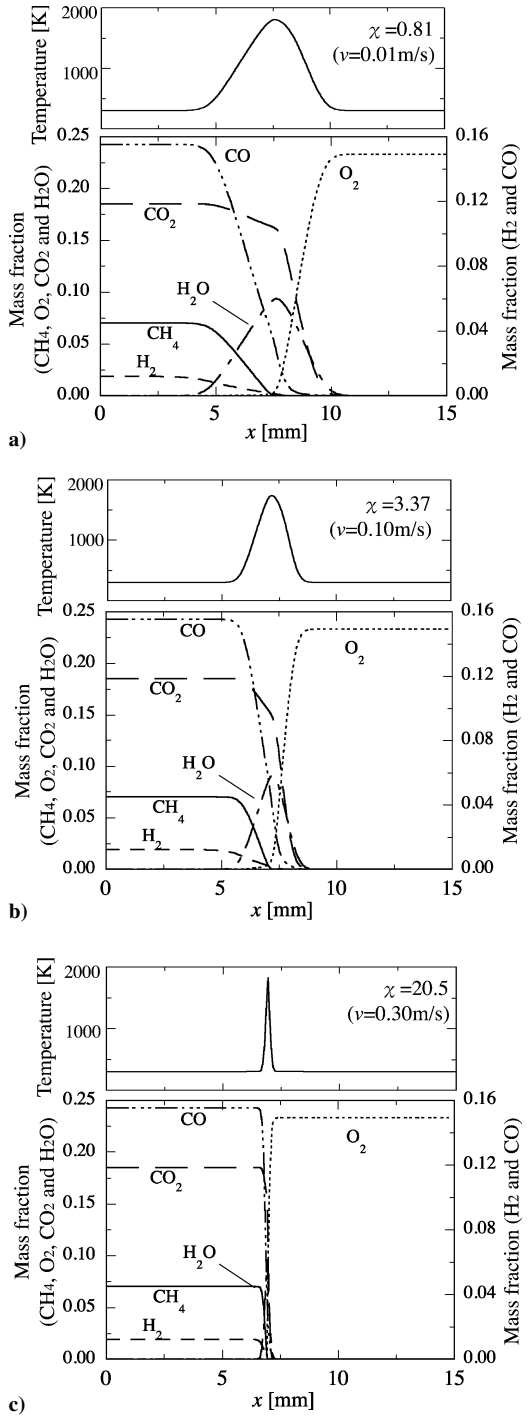

Fig. 3 Examples of counterflow diffusion flame calculations: a) χ = 0.81 1/s, b) χ = 3.37 1/s, and c) χ = 205.2 1/s.

Thermal NO

The thermal NO formation rate is estimated by the Zeldovich mechanism. With a steady-state approximation for a nitrogen atom and by not considering the reverse reaction that is presumed to be in equilibrium, the instantaneous formation rate of NO is represented by[31]

$$\frac{\mathrm{d[NO]}}{\mathrm{d}t} = \upsilon_{\mathrm{NO},T} = A_T[\mathrm{N_2}][\mathrm{O}]\exp\left(\frac{-E_T}{T}\right) \tag{7}$$

where $A_T = 5.74 \times 10^{14}$ (cm^3/mol)$^{1/2}$/s and $E_T = 66{,}900$ K.

Prompt NO

The Fenimore mechanism is closely related to the hydrocarbon combustion chemistry. The general scheme of the Fenimore

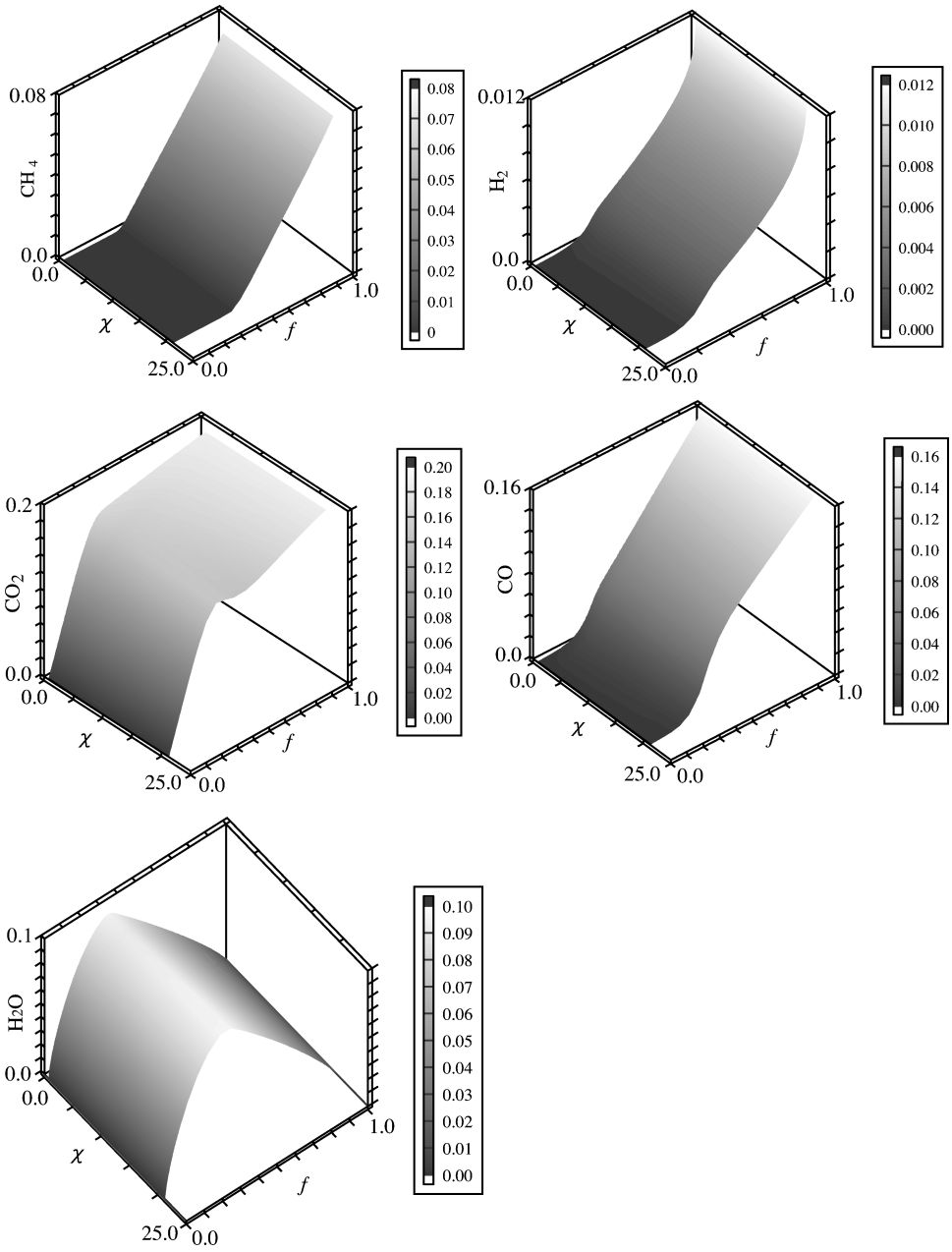

Fig. 4 LHVF flamelet libraries of CH_4, H_2, CO, CO_2, and H_2O.

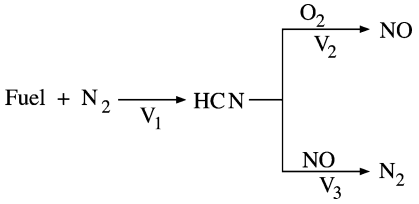

Fig. 5 Prompt NO formation model.

mechanism is that the hydrocarbon radicals react with molecular nitrogen to form amines or cyano compounds. The amines and cyano compounds are then converted into intermediate compounds that ultimately form NO.

In this paper, the prompt NO formation model, as shown in Fig. 5 is newly devised by taking into account the Fenimore mechanism. This model assumes that HCN is formed as an intermediate compound by the reaction between hydrocarbon and atmospheric N_2, and HCN then is either oxidized to NO or converted to N_2 by a reaction with NO.[32] Following DeSoete,[33] the overall reaction rates $v_i (i = 1, 2, 3)$ mol/(m^3 s) are given by

$$v_1 = \rho A_p X_{\text{fuel}}^{0.9} X_{\text{N}_2} \exp(-30{,}000/RT)/M_m \tag{8}$$

$$v_2 = \rho(1 \times 10^{10}) X_{\text{HCN}} X_{\text{O}_2}^{b} \exp(-67{,}000/RT)/M_m \tag{9}$$

$$v_3 = \rho(3 \times 10^{12}) X_{\text{HCN}} X_{\text{NO}} \exp(-60{,}000/RT)/M_m \tag{10}$$

where X_i (i = fuel, N_2, O_2, HCN, and NO) is the mole fraction, M_m kg/kg mol is the molecular weight of mixture, and A_p ($= 1 \times 10^3$) is the model parameter.[32] Here b is the order of the reaction, which varies according to the O_2 mole fraction as follows:

$$b = \begin{cases} 1.0 & (X_{\text{O}_2} \le 0.0037) \\ -0.594 \log(X_{\text{O}_2}) - 2.325 & (0.0037 < X_{\text{O}_2} \le 0.0183) \\ 0.05 & (X_{\text{O}_2} > 0.0183) \end{cases} \tag{11}$$

Overall Formation Rate of NO

NO is normally present only in trace quantities; therefore, the NO formation and LHVF combustion field can be calculated separately.

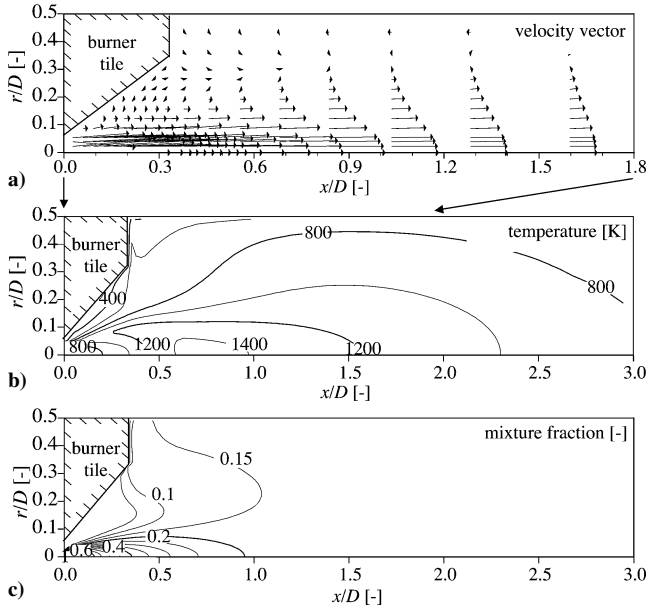

Fig. 6 Calculated results of velocity vectors diagram and contour maps of temperature and mixture fraction.

Equations (7–10) represent the instantaneous laminar rates; it is necessary to time average these equations to obtain the time-mean values of the rate in turbulent flames. This study employs a PDF of the mixture fraction f and scalar dissipation rate χ. The distributions of f and χ are obtained by solving the conservation equations ($\phi = f$ and g) and Eq. (4). Finally, the NO formation is calculated as follows:

$$\bar{v}_{\mathrm{NO},T} = \int_0^1 v_{\mathrm{NO},T}(f,\chi)\cdot\mathcal{P}(f,\chi)\,\mathrm{d}f \tag{12}$$

$$\bar{v}_i = \int_0^1 v_i(f,\chi)\cdot\mathcal{P}(f,\chi)\,\mathrm{d}f \qquad (i=1,2,3) \tag{13}$$

$$\bar{v}_{\mathrm{NO},P} = \bar{v}_2 - \bar{v}_3 \tag{14}$$

$$S_{\mathrm{NO}} = (\bar{v}_{\mathrm{NO},T} + \bar{v}_{\mathrm{NO},P})M_{\mathrm{NO}} \tag{15}$$

$$S_{\mathrm{HCN}} = (\bar{v}_1 - \bar{v}_2 - \bar{v}_3)M_{\mathrm{HCN}} \tag{16}$$

where M_{NO} and M_{HCN} are the molecular weights of NO and HCN, respectively. S_{NO} and S_{HCN} kg/(m^3 s) are the source terms of the conservation equations for the mass fractions of NO and HCN [$\phi = m_{\mathrm{NO}}$ and m_{HCN} in Eq. (1)].

Boundary Conditions

The boundary conditions are as shown in Table 4. The gas flow at the wall boundary is characterized by wall function model. The

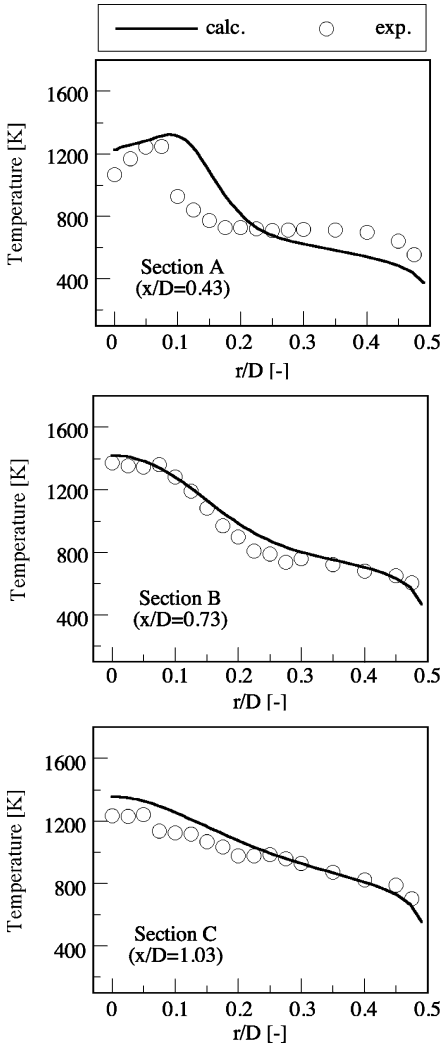

Fig. 7 Comparisons between calculated and measured radial temperature profiles.

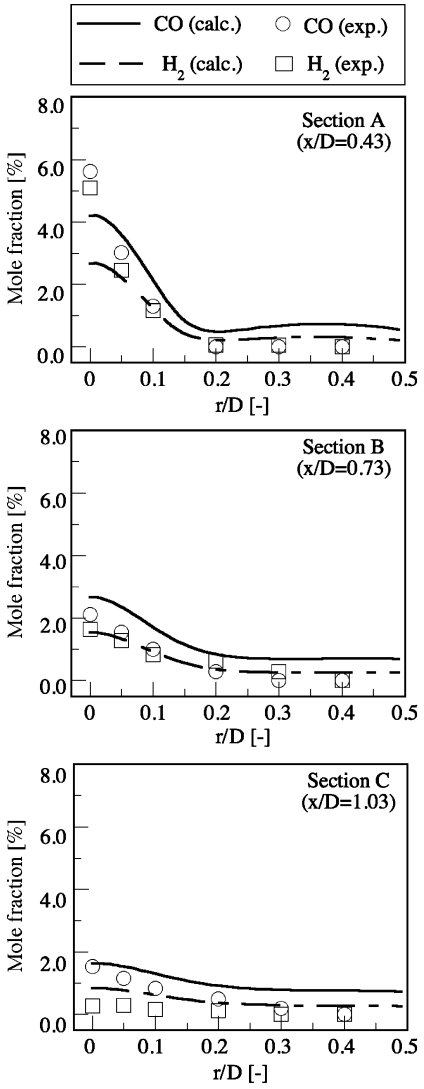

Fig. 8 Comparisons between calculated and measured radial profiles: CO and H_2.

Table 4 Boundary conditions

ϕ	Symmetrical axis	Wall	Outlet plane
U	$\partial U/\partial r = 0$	Wall function	$\partial U/\partial x = 0$
V	0	Wall function	$\partial V/\partial x = 0$
W	$\partial W/\partial r = 0$	Wall function	$\partial W/\partial x = 0$
k	$\partial k/\partial r = 0$	Wall function	$\partial k/\partial x = 0$
ϵ	$\partial \epsilon/\partial r = 0$	Wall function	$\partial \epsilon/\partial x = 0$
h	$\partial h/\partial r = 0$	Heat-balance for wall	$\partial h/\partial x = 0$
f	$\partial f/\partial r = 0$	Wall function	$\partial f/\partial x = 0$

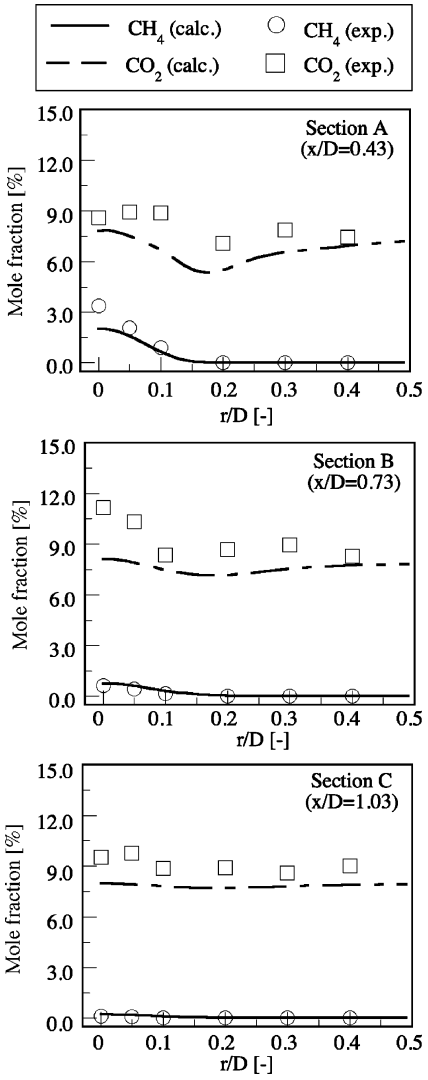

Fig. 9 Comparisons between calculated and measured radial profiles: CO_2 and CH_4.

inner wall temperature of the combustor is estimated by solving the heat-balance equation for the combustor wall. The heat conduction of the wall and heat flux transported to the inner wall by convection and radiation from combustion gas are considered in the equations. The temperature of the outer wall was assumed to be constant (<373 K). LHVF and air inlet velocities, component, temperature, and equivalence ratios are given by experimental conditions.

Result and Discussions

The LHVF flame in the experiments of this study is not luminous throughout the flame region. In addition, the flame has a high stability, and there is no intermittent blowoff. From these observations, we can conclude that the LHVF flame combustion condition in this experiment is fairly good.

The simulation results of the combustion gas velocity vectors and the contour maps of the temperature and mixture fraction are shown in Fig. 6. The outer recirculation zone is clearly visible, and the area of the mixture fraction $f = 0.15$ spreads widely in the upstream region of the combustor. This implies that the burned gases in the downstream region are transported to the upstream region by the outer recirculation flow. With regard to the temperature contour map, a rapid temperature increase occurs in the vicinity of the injector, and a high-temperature region ($\approx$1400 K) is created around $x/D = 0.8$.

Figure 7 shows the comparisons between the measured and simulated radial temperature profiles in each position. These calculations are in good agreement with the measured results of temperature at positions B and C. However, at position A the calculated temperature is overestimated compared with that obtained in experiments in the center region.

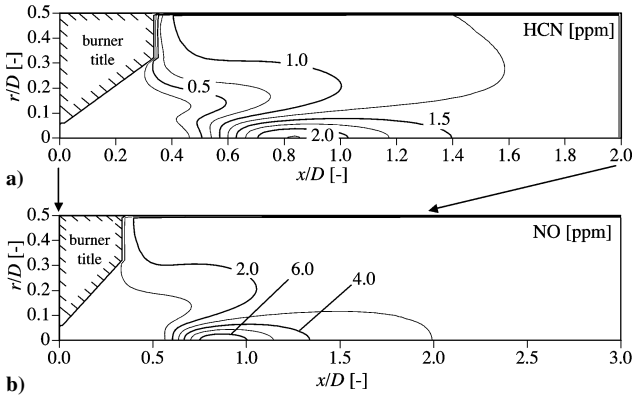

Fig. 10 Calculated contour maps of NO and HCN.

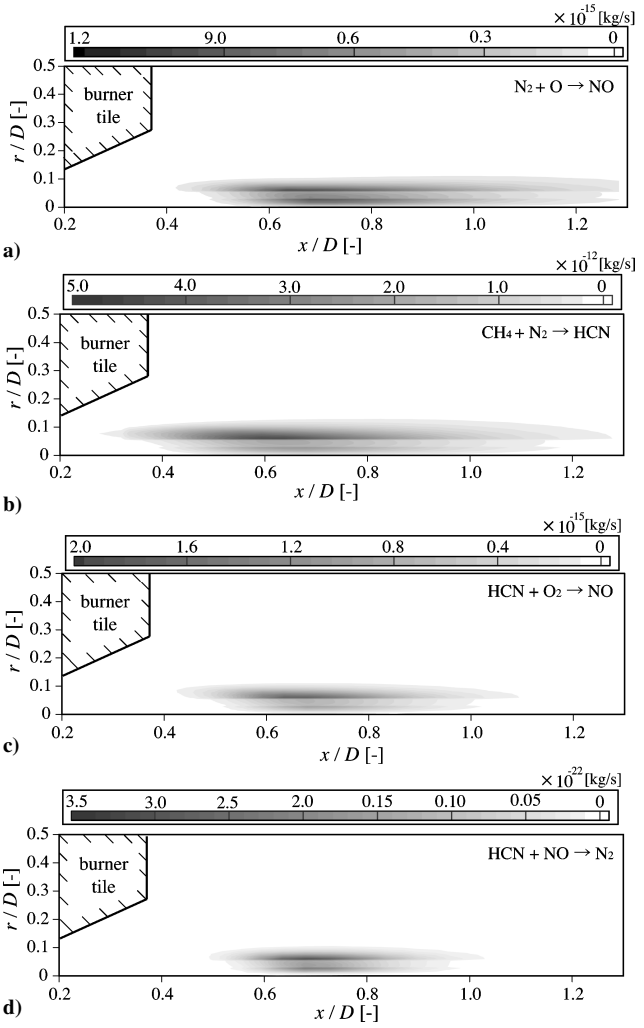

Fig. 11 Contour maps of the reaction rates of NO and HCN formation and deformation.

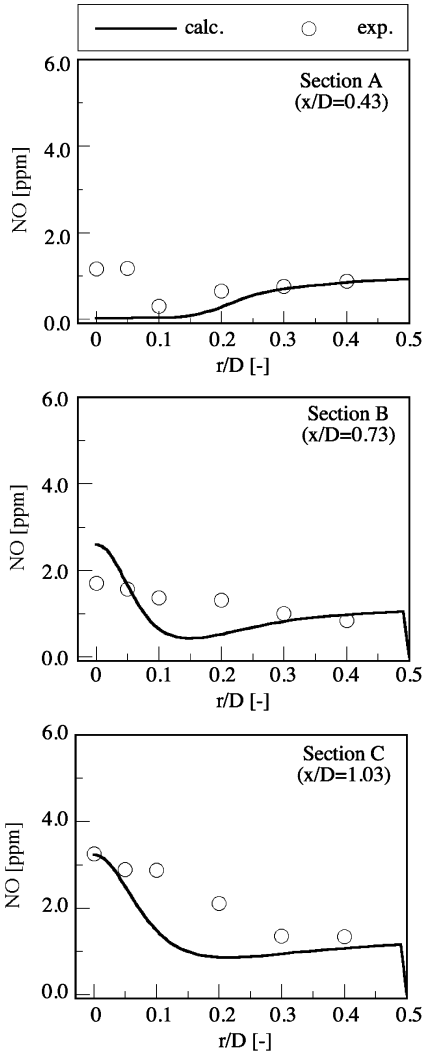

Fig. 12 Comparisons between calculated and measured radial profiles of NO.

Figure 8 shows radial profiles of the combustible specie concentrations of H_2 and CO. In position A, the measured profiles of H_2 and CO show peaks near the centerline of the combustor. These peaks decrease at position B and do not appear at position C. The calculated profiles of H_2 and CO appear to be slightly underestimated for small radii ($r/D < 0.1$) at position A and overestimated for large radii ($r/D > 0.2$) at all positions. These discrepancies are prominent in the CO profile.

Figure 9 shows the radial concentration profiles of CO_2 and CH_4 at each position. The measured CH_4 is prominent at position A; however, this is not the case at position B. This tendency is predicted to a significant extent by the calculations, although its value is underestimated for small radii at position A. By comparing the CH_4 profiles with that of CO and H_2 in Fig. 8, it can be considered that CH_4 is burned and decomposed in the early stage of LHVF combustion. This consideration is followed by our previous study,[28] which simulated the LHVF counterflow diffusion flame using a detailed reaction mechanism (49 chemical species and 279 element reactions). Considering the measured CO_2 profiles in position A, there is a dip at $r/D = 0.2$. This tendency implies that the boundary is formed by jet flows from the injector and the outer recirculation flow. The calculated CO_2 profile predicts this boundary with a high degree of accuracy.

It is expected that the discrepancies in temperature and chemical species concentrations just stated are caused by the accuracy of the k-ϵ turbulent model rather than that of the flamelet turbulent combustion model. However, the calculated results could approximately predict the measured results. Thus, the combination of the k-ϵ turbulent model and the flamelet turbulent combustion model with the flamelet library created in this paper is useful for the numerical simulation of the LHVF gas turbine combustor.

Figure 10 shows simulated contour maps of the NO and HCN concentrations. The contour maps of the reaction rates of NO and HCN are shown in Fig. 11. Comparing with the both the NO and HCN distributions on the central axis, HCN is found to have generated in the upstream of the region where NO is generated. This result agrees well with those of previous researches that HCN is the source of NO formation at the beginning of the combustion reaction.[31,34]

Figure 12 shows the comparisons of the measured and simulated radial NO concentration profiles. The simulated NO concentration is underestimated at small radii ($r/D < 0.1$) at each position. These discrepancies in NO formation can be attributed to the calculation accuracies of the combustion gas temperature and flow. However, the quantitative agreement between the measurements and calculations is fairly good at all positions.

Conclusions

This study developed a turbulent LHVF combustion simulation model for industrial and practical uses. A k-ϵ two-equation model was used as a turbulent flow model, and a flamelet model with a flamelet library specialized in LHVF combustion was employed as a combustion model. In addition, the newly developed NO formation model takes into account the PDF as well as the Zeldovich and Fenimore mechanisms. The emphases of the model are in predicting the thermal and prompt NO separately; the HCN formed as an intermediate of the combustion reaction and the sources of NO formation. Based on the comparison between measured and simulated results, it is clear that the LHVF flamelet model can be used to calculate the turbulent combustions within reason. In particular the tendencies of the calculated results of temperature and chemical species show good agreement with the experimental results. In addition, the calculated NO concentration shows good agreement quantitatively.

From these results and comparisons, the authors concluded that both the numerical simulation models of the turbulent LHVF combustion and the NO formation are effective tools for simulating the LHVF turbulent combustion field and designing the LHVF gas turbine combustor. The applicability of this simulation model to other LHVF having compositions different from that in this study is the next task of this study.

References

[1]Cavaliere, A., and de Joannon, M., "Mild Combustion," *Progress in Energy and Combustion Science*, Vol. 30, No. 4, 2004, pp. 329–366.

[2]Arai, N., Teramae, N., and Kobayashi, N., "R&D Trends in Gas Turbine," *Energy World*, Vol. 226, No. 2, 1995, pp. 16, 17.

[3]Yamamoto, T., Miyazaki, T., Furuhata, T., Arai, N., Kobayashi, N., and Miura, T., "Temperature Profile in the Pressurized Methane-Air Combustor," *Journal of Flow Visualization and Image Processing*, Vol. 5, No. 1, 1998, pp. 51–62.

[4]Yamamoto, T., Furuhata, T., and Arai, N., "Thermodynamic Analysis and Optimization of New Concept Combined Cycle 'Chemical Gas Turbine' System," *International Journal of Applied Thermodynamics*, Vol. 3, No. 4, 2000, pp. 155–162.

[5]Yamamoto, T., Furuhata, T., Arai, N., and Mori, K., "Thermodynamic Analysis of Gas Turbine System Using Fuel Rich and Lean Combustions," *Proceedings of the 6th World Congress of Chemical Engineering*, edited by D. Wood, AICHE, No. 1, 2001, p. 118.

[6]Jones, W. P., and Whitelaw, J. H., "Modeling and Measurements in Turbulent Combustion," *Proceedings of the 21st Symposium (International) on Combustion*, Combustion Inst., Pittsburgh, PA, No. 1, 1984, pp. 233–249.

[7]Datta, A., and Som, S. K., "Combustion and Emission Characteristics in a Gas Turbine Combustor at Different Pressure and Swirl Conditions," *Applied Thermal Engineering*, Vol. 19, No. 2, 1999, pp. 949–996.

[8]Grandinger, B. T., Inauen, A., Bombach, R., Kappeli, B., Hubschmid, W., and Boulouchos, K., "Liquid-Fuel/Air Premixing in Gas Turbine Combustors: Experiment and Numerical Simulation," *Combustion and Flame*, Vol. 123, No. 3, 2001, pp. 422–443.

[9]Yaga, M., Sasada, K., Yamamoto, T., Aoki, H., and Miura, T., "An Eddy Characteristic Time Modeling in LES for Gas Turbine Combustor," *Proceedings of the International Joint Power Generation Conference* [CD-ROM], ASME, IJPGC 2000-15042, 2000.

[10]Yaga, M., Sasada, K., Yamamoto, T., Aoki, H., and Miura, T., "Modeling of Eddy Characteristic Time in LES for Calculating Turbulent Diffusion

Flame," *International Journal of Heat and Mass Transfer*, Vol. 45, No. 11, 2002, pp. 2343–2349.

[11]Torii, S., "Numerical Simulation of Turbulent Jet Diffusion Flames by Means of Two-Equation Heat Transfer Model," Vol. 42, No. 15–17, 2001, pp. 1953–1962.

[12]Makita, T., Miyazaki, T., Furuhata, T., and Arai, N., "Turbulent Combustion Characteristics of a Pressurized Methane-Air Combustor Under Fuel-Rich Conditions," *Proceedings of the International Joint Power Generation Conference* [CD-ROM], ASME, IJPGC 2000-15048, 2000.

[13]Makita, T., Yamamoto, T., Furuhata, T., and Arai, N., "Numerical Simulation of High-Pressure and Fuel-Rich Turbulent Combustion Field," *Journal of Propulsion and Power*, Vol. 19, No. 2, 2003, pp. 226–234.

[14]Chomiak, J., Longwell, J. P., and Sarofim, A. F., "Combustion of Low Calorific Value Gases; Problems and Prospects," *Progress in Energy and Combustion Science*, Vol. 15, No. 1, 1989, pp. 109–129.

[15]Choi, G. M., and Katsuki, M., "New Approach to Low Emission of Nitric Oxides from Furnaces Using Highly Pre-Heated Air Combustion," *Journal of the Institute of Energy*, Vol. 73, No. 1, 2000, pp. 18–24.

[16]Launder, B. E., "Turbulent Flow Modeling," *International Journal of Heat and Mass Transfer*, Vol. 15, No. 3, 1972, pp. 301–309.

[17]Patanker, S. V., and Spalding, D. B., "A Computer Model for Three-Dimensional Flow in Furnaces," *Proceedings of the 14th Symposium (International) on Combustion*, Combustion Inst., Pittsburgh, PA, No. 1, 1973, pp. 605–614.

[18]Patanker, S. V., *Numerical Heat Transfer and Fluid Flow*, Hemisphere, New York, 1980, Chap. 4.

[19]Peters, N., "Laminar Diffusion Flamelet Models in Non-Premixed Turbulent Combustion," *Progress in Energy and Combustion Science*, Vol. 10, No. 3, 1984, pp. 319–339.

[20]Chen, P. C., Yeh, Y. C., Clement, G. Y., and Kenneth, D. M., "Numerical Modeling of NO Formation in Laminar Bunsen Flames: A Flamelet Approach," *Combustion and Flame*, Vol. 114, No. 3–4, 1998, pp. 420–435.

[21]Peters, N., "Laminar Flamelet Concepts in Turbulent Combustion," *Proceedings of the 21th Symposium (International) on Combustion*, Combustion Inst., Pittsburgh, PA, No. 1, 1986, pp. 1231–1250.

[22]Magnussen, B. F., and Hjertager, B. H., "On Mathematical Modeling of Turbulent Combustion with Special Emphasis on Soot Formation and Combustion," *Proceedings of the 16th Symposium (International) on Combustion*, Combustion Inst., Pittsburgh, PA, No. 1, 1976, pp. 719–729.

[23]Liew, S. K., Bray, N. C., and Moss, J. B., "A Flamelet Model of Turbulent Non-Premixed Combustion," *Combustion Science and Technology*, Vol. 27, No. 1, 1981, pp. 69–73.

[24]Lentini, D., and Puri, I. K., "Stretched Laminar Flamelet Modeling of Turbulent Chloromethane-Air Nonpremixed Jet Flames," *Combustion and Flame*, Vol. 103, No. 4, 1995, pp. 328–338.

[25]Janicka, J., and Peters, N., "Prediction of Turbulent Jet Diffusion Flame Lift-off Using a PDF Transport Equation," *Proceedings of the 19th Symposium (International) on Combustion*, Combustion Inst., Pittsburgh, PA, No. 1, 1982, pp. 367–374.

[26]Yamashita, H., Nishioka, M., and Takeno, T., "Prediction of NO_x Production Rate in the Turbulent Diffusion Flame," *Energy Conversions and Management*, Vol. 38, No. 10–13, 1997, pp. 1343–1352.

[27]Bendtsen, A. D., Glarborg, P., and Johansen, D. K., "Chemometric Analysis of a Detailed Chemical Reaction Mechanism for Methane Oxidation," *Chemometrics and Intelligent Laboratory Systems*, Vol. 44, No. 1–2, 1998, pp. 353–361.

[28]Fujiwara, Y., Yamamoto, T., Furuhata, T., and Arai, N., "Combustion Characteristics and Numerical Simulations of Low Heat-Value Fuel During Highly Preheated Air Combustion," *Proceedings of the 4th International Symposium on High Temperature Air Combustion and Gasification (HTACG)*, edited by K. Yoshikawa, Vol. 1, ENEA, Roma, 2001, pp. 26–30.

[29]Fisher, E. M., and Koshland, C. P., "Numerical Simulation of the Thermal Destruction of Some Chlorinated C1 and C2 Hydrocarbons," *Journal of the Air and Waste Management*, Vol. 46, No. 10, 1990, pp. 1384–1390.

[30]Smooke, D. M., and Giovangigli, V., "NO Production in the Couterflow Diffusion Flame," *Modeling in Combustion Science*, Vol. 1, No. 1, 1995, pp. 81–106.

[31]Turns, R. S., *An Introduction to Combustion*, McGraw–Hill, New York, 1996, Chap. 5.

[32]Furuhata, T., Tanno, S., Miura, T., Ikuno, T., Abe, T., Sugimoto, T., and K. U., "Prediction of NO Concentration in a Liquid-Fueled Gas Turbine Combustor," *Transport Phenomena in Combustion*, Vol. 2, No. 3, 1995, pp. 1271–1282.

[33]DeSoete, G. G., "Overall Reaction Rate of NO and N_2 Formation from Fuel Nitrogen," *Proceedings of the 15th Symposium (International) on Combustion*, Combustion Inst., Pittsburgh, PA, No. 1, 1979, pp. 1093–1102.

[34]Kuo, K. K., *Principles of Combustion*, Wiley, New York, 1986, Chap. 6.